

## MIT Open Access Articles

*Hysteresis from Multiscale Porosity: Modeling Water Sorption and Shrinkage in Cement Paste*

The MIT Faculty has made this article openly available. **Please share** how this access benefits you. Your story matters.

**Citation:** Pinson, Matthew B., et al. "Hysteresis from Multiscale Porosity: Modeling Water Sorption and Shrinkage in Cement Paste." *Phys. Rev. Applied* 3, 064009 (June 2015). © 2015 American Physical Society

**As Published:** <http://dx.doi.org/10.1103/PhysRevApplied.3.064009>

**Publisher:** American Physical Society

**Persistent URL:** <http://hdl.handle.net/1721.1/97464>

**Version:** Final published version: final published article, as it appeared in a journal, conference proceedings, or other formally published context

**Terms of Use:** Article is made available in accordance with the publisher's policy and may be subject to US copyright law. Please refer to the publisher's site for terms of use.





# Hysteresis from Multiscale Porosity: Modeling Water Sorption and Shrinkage in Cement Paste

Matthew B. Pinson

*Department of Physics, Massachusetts Institute of Technology, Cambridge, Massachusetts 02139, USA*

Enrico Masoero

*School of Civil Engineering and Geosciences, Newcastle University,  
Newcastle upon Tyne NE1 7RU, United Kingdom*

Patrick A. Bonnaud

*New Industry Creation Hatchery Center, Tohoku University, Sendai 980-8578, Japan*

Hegoi Manzano

*Molecular Spectroscopy Laboratory, Universidad del País Vasco/EHU, 48080 Bilbao, Spain*

Qing Ji

*Inspur Group, State Key Laboratory of High-End Server & Storage Technology,  
Jinan, Shandong 250101, People's Republic of China*

Sidney Yip

*Department of Nuclear Science and Engineering, Massachusetts Institute of Technology,  
Cambridge, Massachusetts 02139, USA*

Jeffrey J. Thomas

*Schlumberger-Doll Research, Cambridge, Massachusetts 02139, USA*

Martin Z. Bazant

*Department of Chemical Engineering and Department of Mathematics,  
Massachusetts Institute of Technology, Cambridge, Massachusetts 02139, USA*

Krystyn J. Van Vliet

*Department of Materials Science and Engineering and Department of Mechanical Engineering,  
Massachusetts Institute of Technology, Cambridge, Massachusetts 02139, USA*

Hamlin M. Jennings\*

*Department of Civil and Environmental Engineering, Massachusetts Institute of Technology,  
Cambridge, Massachusetts 02139, USA*

(Received 2 September 2014; revised manuscript received 29 January 2015; published 17 June 2015)

Cement paste has a complex distribution of pores and molecular-scale spaces. This distribution controls the hysteresis of water sorption isotherms and associated bulk dimensional changes (shrinkage). We focus on two locations of evaporable water within the fine structure of pastes, each having unique properties, and we present applied physics models that capture the hysteresis by dividing drying and rewetting into two related regimes based on relative humidity (RH). We show that a continuum model, incorporating a pore-blocking mechanism for desorption and equilibrium thermodynamics for adsorption, explains well the sorption hysteresis for a paste that remains above approximately 20% RH. In addition, we show with molecular models and experiments that water in spaces of  $\lesssim 1$  nm width evaporates below approximately 20% RH but reenters throughout the entire RH range. This water is responsible for a drying shrinkage hysteresis similar to that of clays but opposite in direction to typical mesoporous glass. Combining the models of these two regimes allows the entire drying and rewetting hysteresis to be reproduced accurately and provides parameters to predict the corresponding dimensional changes. The resulting model can improve the engineering predictions of long-term drying shrinkage accounting also for the history dependence of strain induced by hysteresis. Alternative strategies for quantitative analyses of the

\*Corresponding author.  
hmj@mit.edu

microstructure of cement paste based on this mesoscale physical model of water content within porous spaces are discussed.

DOI: [10.1103/PhysRevApplied.3.064009](https://doi.org/10.1103/PhysRevApplied.3.064009)

## I. INTRODUCTION

Evaporable water in cement paste influences important mechanical properties such as drying shrinkage [1–3] and creep [4–11]. These influences are due to forces that water and dissolved ions exert from within the complex, multiscale pore system that develops during hydration, i.e., after dry cement powder (mostly calcium silicate minerals) reacts with water. The size, distribution, and connectivity of the pores are largely determined by the precipitation process of calcium silicate hydrate (C–S–H), a semicrystalline and nonstoichiometric solid with layered molecular structure that may be modeled as imperfect tobermorite, possibly intermixed with jennite [12–15]. The C–S–H precipitation process forms a material referred to as C–S–H gel [12,16]. This gel comprises a solid network with pore widths of several nanometers. Furthermore, similar to clay, the solid network itself contains evaporable water within its layered molecular structure in spaces  $< 1$  nm [17].

The water sorption isotherm [water content as a function of relative humidity (RH) during drying and rewetting] is potentially a powerful technique to understand changes in this microstructure, as it samples evaporable water at all scales [17–19]. Even more information is obtained by also measuring the bulk-volume change with RH. Understanding the complex behavior of water as it moves in and out of the C–S–H phase can be the key for a new generation of models to predict the dimensional changes of hardened cement paste and the induced stresses resulting from changes in RH. Bulk-volume changes are central to cracking and durability of cement and concrete; hence, models that link these engineering properties to specific microstructural features can offer new ways to perform quality control, assess degradation, and design new cement-based materials. The success of endeavors in this direction is presently limited by physical complexities including (1) the presence of evaporable water in pores at all scales, from molecular to macroscopic, which requires an understanding of the pore-width-specific behavior of water (e.g., evaporation and condensation and associated pressures) and (2) the role played by the connectivity of the pore network across multiple scales in limiting bulk transport of water [20], which requires experimental techniques that can sample sufficiently large volumes of material.

At present, connections between measured sorption isotherms, pore structure, and associated properties rely on models that link the evaporation and condensation of water at a given RH with the width and connectedness of the pores over a range of scales [18,19,21,22]. Models for mesoporous materials are typically extensions of the

Kelvin-Laplace theory, which links the RH with the width of pores being emptied or filled and with the pore pressure causing volumetric strain [23,24]. Such models can capture well the macroscopic sorption and shrinkage behavior of mesoporous materials that display hysteresis only at high RH, for example, that of Vycor® glass [23] in Fig. 1(c). The situation is quite different for cement paste, where a multiscale pore structure leads to hysteresis over the whole range of RH from 0% to 100% [see Fig. 1(a)]. Hysteresis at very low RH is also typical of clays [Fig. 1(b)], where the sorption process is controlled by evaporable water in molecular layers [25,26]. For cement paste, the key role of water in C–S–H molecular layers and other possible molecular-scale spaces is further evidenced by the drying shrinkage behavior [see Figs. 1(d)–1(f)]: as with clay, but in contrast to Vycor porous borosilicate glass, the volume at a given RH is smaller during wetting than during drying, when the experiment is performed over the entire range of RH. A self-consistent model of both sorption and drying shrinkage that captures the hysteresis and explains the difference between cement paste and other mesoporous materials, like Vycor, is still lacking.

Here we propose a mesoscale model of water sorption in cement paste, in which the physical behavior of water in molecular-scale spaces is treated as fundamentally different from that of water in gel and capillary pores. We focus only on the so-called “reversible” part of the material’s response to humidity changes, i.e., the part that is repeatable through successive cycles of drying and wetting. The first drying is, in fact, accompanied by large irreversible microstructural changes that can be significantly affected by creep (see, e.g., Ref. [30]). Reversibility is attained only after a first severe drying, which is unlikely to take place in most practical applications. However, understanding the reversible contribution to the hysteresis is a necessary foundation for future studies of the irreversible mechanisms. To study the reversible water sorption, we first use a variety of published experimental and computational results to estimate the sorption isotherm in the molecular-scale spaces of the C–S–H. This partial isotherm is then subtracted from the entire experimental isotherm for cement paste (second and further sorption cycles), providing a reduced sorption isotherm that includes only the contribution from the gel and capillary pores. The interpretation of this reduced isotherm using traditional theories provides information about the pore network, whereas molecular modeling and simulations [21] and results from nuclear magnetic resonance (NMR) experiments [31] help interpret the partial isotherm associated with the molecular-scale spaces. Based

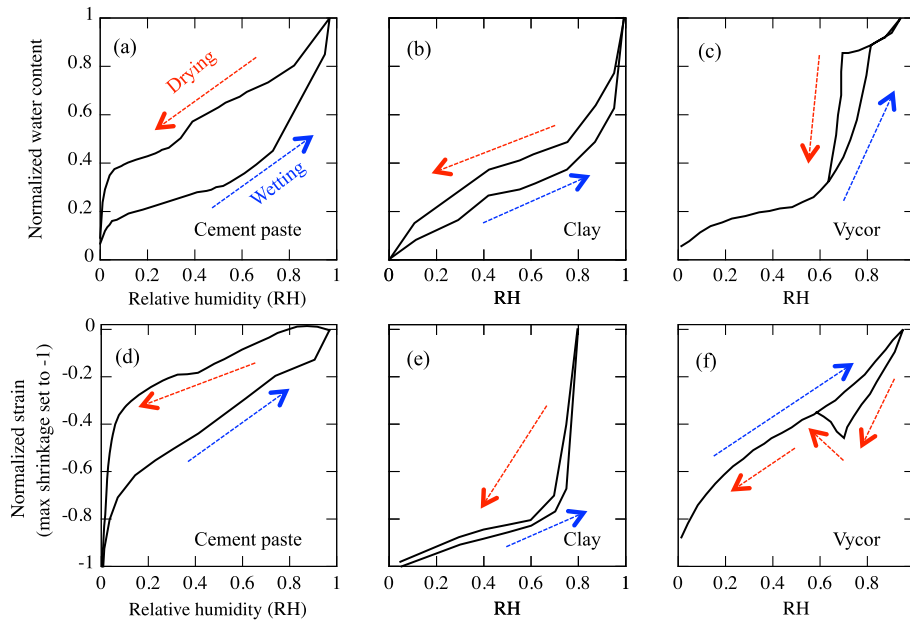


FIG. 1. Water sorption isotherms and corresponding shrinkage for (a), (d) portland cement paste [27], (b), (e) raw clay with calcium ions in the molecular layers [28], and (c), (f) Vycor glass [29]. The shrinkage strain is a volume strain of less than 1% for cement paste and Vycor and more than 10% for clay. Here our focus is on the behavioral similarity between cement paste and clay as opposed to Vycor glass; the latter is a typical example of mesoporous material for which water molecules do not enter the molecular structure of the solid network. Notice that the drying (red) and wetting (blue) strain paths for cement paste and clay (d), (e) are opposite (upside down) compared to those of Vycor (f).

on this new combined approach, we propose a simple physical model that translates microstructural information from the sorption isotherm into a correct prediction of the (reversible) drying shrinkage of cement paste over the whole range of RH. Finally, we discuss promising directions of future research as well as implications for other properties of cement paste important in applied physics and engineering problems.

## II. CLASSIFICATION OF WATER IN CEMENT PASTE

We divide water into four categories based on its local environment within the microstructure, driven by the observed physical properties. Where possible, we maintain traditional nomenclature. Specifically, we propose that the isotherm in Fig. 1(a) can be modeled as the sum of several processes and that macroscale dimensional changes upon drying or rewetting are the sum of the responses as each of these categories of water enters and leaves the structure. Note that in this paper, we refer to the aqueous fluid within the pores as water when, in fact, it is an electrolyte of water with dissolved ions. Our approach and nomenclature are summarized in Fig. 2.

- (1) Interlayer water in spaces with width  $\lesssim 1$  nm. Molecular water in this type of space is bound strongly and is removed only at low RH. Traditionally, interlayer water is defined as residing between the silicate-rich layers of solid C—S—H, integral to

the structure of the solid. Here we broaden the definition to include water in any space of below approximately 1 nm in width with a similar chemical and physical environment for water molecules; i.e., the water is in contact with atomistically rough surfaces built from silicate tetrahedra with nonhydroxylated dangling oxygen atoms. These spaces include those caused by defective stacking between layers, as well as contact regions where C—S—H regions (or particles) with different crystallographic orientations are in close proximity (see Fig. 2). Molecular simulations and experiments (described in detail in a later section) indicate that water does not evaporate from these spaces until RH is decreased below 20%. It is well documented [17,32] that there is substantial collapse and swelling of the interlayer space as water is removed and reinserted, respectively. In other words, the insertion of water into the interlayer space confers a mechanical disjoining effect.

- (2) Water in gel pores with widths between approximately 1 and 10 nm. Gel porosity is defined in the literature as the minimum amount of porosity that can be achieved in a cement paste, i.e., that resulting from conditions under which the capillary pores are replaced by reaction products that fill the original water-filled space [33]. In this definition, the interlayer spaces are not included as porosity. The lower size limit of 1 nm corresponds to the upper limit of the interlayer space (described above).

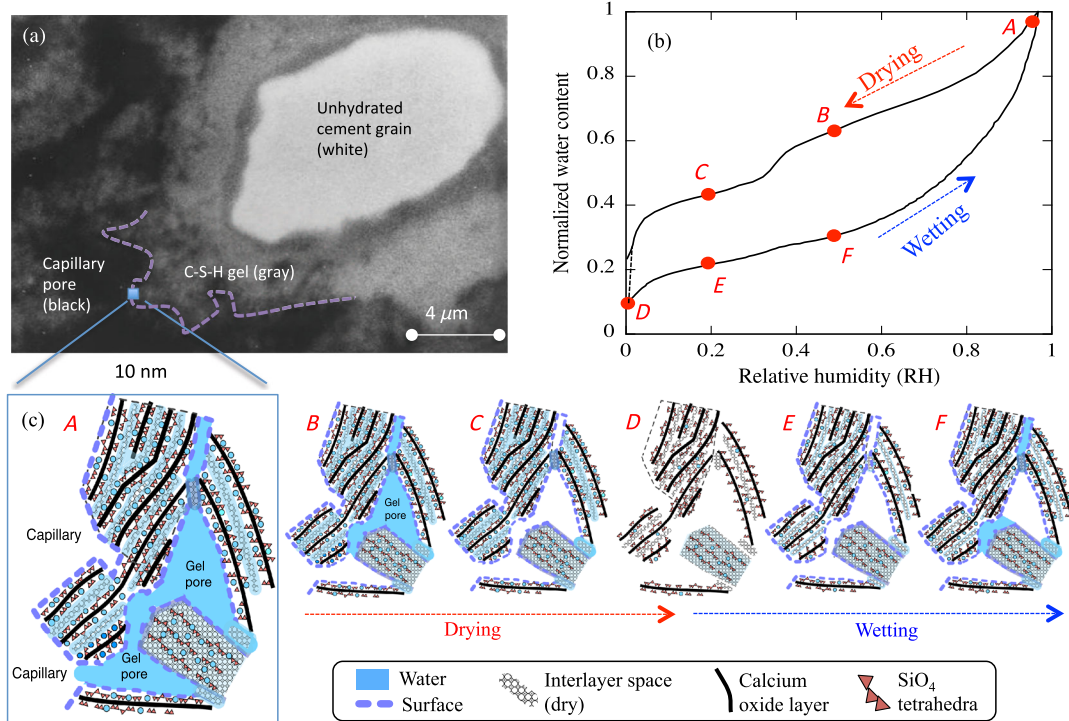


FIG. 2. Schematic of a C–S–H gel structure during a drying and wetting cycle. (a) Backscattered scanning electron micrograph of a polished cement paste surface. (b) water sorption isotherm from Fig. 1(a) with six points marked A–F. (c) Schematic diagrams illustrating the C–S–H water content at the same six points. These diagrams illustrate the two independent hystereses in the gel pores and interlayer space that are combined to reproduce the overall observed isotherm. (A) Saturated state with large capillary pores empty, which is the reference configuration used in this paper (see text). (B) and (F) show configurations at the same intermediate RH but different water content in the gel pores. Water leaves the gel pores during drying to 15% RH, governed by pore blocking, and reenters during wetting, governed by equilibrium. (C) and (E) show configurations at the same low RH with different water content within interlayer space. (D) shows an almost completely dried configuration. Note that different regions of C–S–H have different orientations of the molecular layers (texture).

- (3) Water in capillary pores with width greater than 10 nm. These pores are responsible for the hysteresis between drying and rewetting above 85% RH [17,34]. NMR experiments [31] show that 85% RH is a relevant threshold value for the capillary pores to be empty, and the Kelvin equation provides the corresponding pore width of 10 nm. The Kelvin equation also indicates that empty pores greater than 100 nm can fill only at RH very close to 100% in equilibrium conditions. The filling of such pores is difficult unless the sample is immersed; hence, pores of greater than 100 nm can be considered devoid of condensed water and simply lined with a thin shell of adsorbed water. Finally, we acknowledge the ongoing debate regarding whether small capillary pores with width between 10 and 100 nm are intrinsic to the formation of the C–S–H gel itself or leftover space from incomplete filling during hydration [18,35]; in any case, the origin of these pores does not affect our models or results.
- (4) Surface-adsorbed water in empty pores. This is defined as the water present in gel and capillary pores after pores are empty of bulk water, present as a

thin adsorbed layer on the walls. This adsorbed water is influential in determining shrinkage because it affects the surface energy of the solid-pore interface.

Based on the above, we suggest that the solid component of the C–S–H phase, which we define to include not only the C–S–H layers but also the interlayer space, will have constant water content and, therefore, nearly constant structure and mechanical properties as long as the RH is never reduced below approximately 25%. This constancy is implied because the interlayer water will remain present, as shown via molecular-scale simulations, as discussed below. Under these conditions only, cement paste behaves like a simple mesoporous material such as Vycor glass.

### III. MODELING THE WATER SORPTION ISOTHERM

#### A. Model description

We explain the sorption behavior of cement paste using a multistep modeling approach that accounts for the behavior of water in each of the different spaces described above. We begin by estimating the interlayer water contribution to the isotherm and subtracting it from the experimental isotherm.

We then use the adsorption branch of the resulting reduced isotherm to compute iteratively the pore-width distribution and the surface area of gel and capillary pores.

### 1. Interlayer water

The first step toward understanding the sorption isotherm is to isolate the contribution of interlayer water, which does not evaporate until very low RH. Since direct experimental measurements of interlayer water content upon adsorption are not yet available, we first estimate this water content based on one of the present authors' analysis [17] of published experimental data by Feldman [36]. To experimentally determine the interlayer water content on the adsorption branch at a particular RH  $h$ , the sample is first fully dried to 0% RH, then equilibrated at  $h$ . This procedure ensures that the interlayer water content reaches (local) equilibrium at  $h$ , and for sufficiently high  $h$ , it will also result in some water being present in the gel pores. The RH is then decreased from  $h$  down to a level at which the gel pores are empty of condensed water: in this case, 11% [36].

From the water that remains, the quantity adsorbed on pore walls must be subtracted: this quantity is estimated as 0.25 moles per mole of C—S—H [17]. The result is the interlayer water content at  $h$ , which is plotted in Fig. 3(c).

During desorption, the interlayer water is removed below a threshold RH. We assume for simplicity that this water is removed linearly as RH is reduced from 15% to 0%; see Appendix D for further discussion of this linearity assumption. The 15% RH threshold differs slightly from the reference point of 11% described above, which is based on an estimate of the RH at which the adsorbed layer on the pore surface is one molecule thick [37,38], not specifically on a threshold between gel pore and interlayer water removal. The existence of a threshold RH for interlayer water desorption is supported by some of the present authors' molecular-scale simulations [21,22], as shown in Figs. 3(a)–3(c) and by NMR experiments [31], as shown in Fig. 3(c). The NMR experiments provide information on characteristic relaxation times of water in cement paste, which then are correlated to the amount of water in different

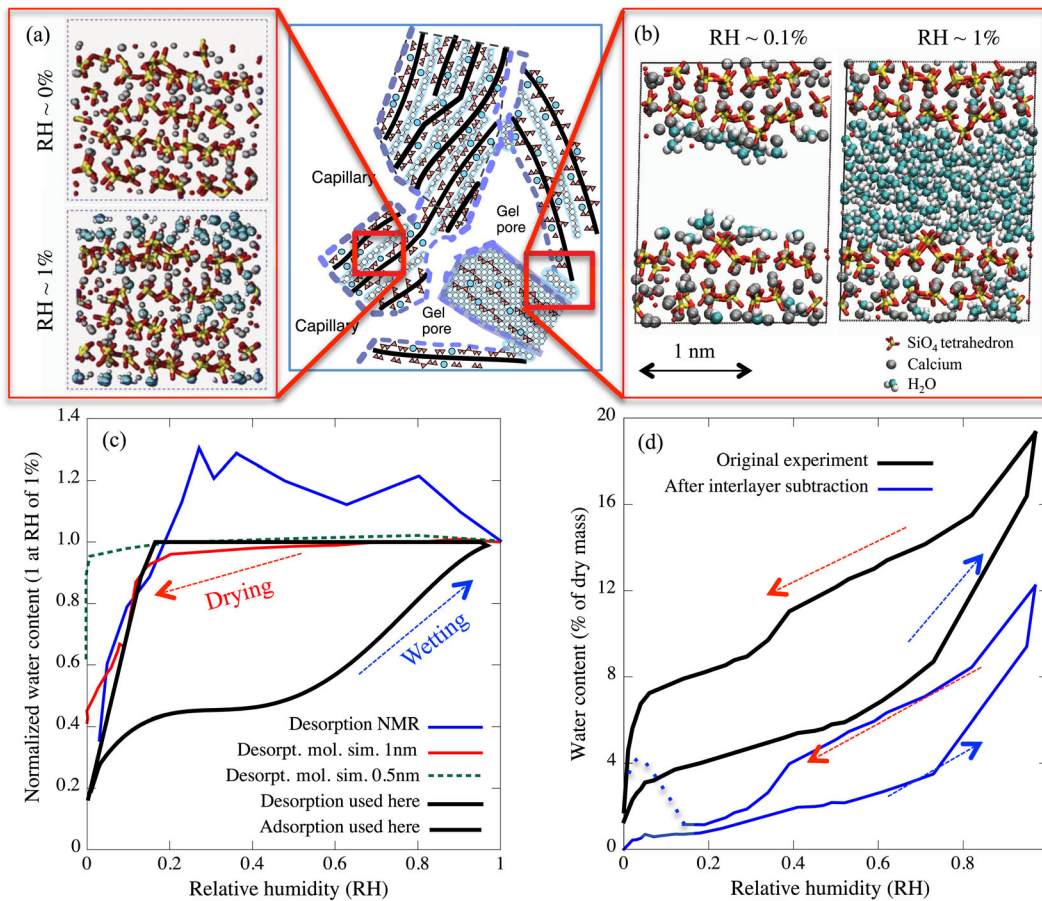


FIG. 3. Simulated water content of a (a) 0.5-nm and a (b) 1-nm interlayer space at low and high RH. (c) Estimate of interlayer water content as a function of RH using our simple assumption of removal below 15% RH and adsorption from indirect experimental evidence based on scanning isotherms (black), NMR data [31] (blue), and molecular simulations [21,22] (red, green). NMR data indicate an apparent increase of water content when desorbing at large RH: this effect has been attributed in Ref. [31] to the emptying of gel pores that leave a surface layer of water that the experiment cannot distinguish from interlayer water. (d) Original isotherm from Feldman and Sereda [27] and reduced isotherm obtained by subtracting the interlayer water isotherm.

pore categories at given environmental RH, including the interlayer water shown in Fig. 3. Molecular simulations of water content, using the grand canonical Monte Carlo (GCMC) approach to predict the number of water molecules at specific chemical potentials (and, thus, specific imposed RH), indicate that water does not desorb from C—S—H interlayer spaces of approximately 1 nm width until approximately 15% RH [22]. As RH is decreased further to 0%, these water molecules desorb, and the C—S—H unit cells increasingly densify. These simulations describe two types of interlayer spaces of width 0.5 and 1 nm [Figs. 3(a) and 3(b)]. The smaller width corresponds to what are also known in the literature as “intragranular” C—S—H layers [21], while a 1 nm distance between silicate-rich layers exceeds that expected for a C—S—H unit cell [39] and is termed “intergranular.” However, our current definition of interlayer space as regions between silicate-rich layers that are smaller than a gel pore does not further distinguish between these two types of nanometer-scale interlayer spaces when computing interlayer water content and its impact on isotherms or drying shrinkage. Interlayer water content during wetting has also been calculated using GCMC simulations [22], but since these simulations do not yet account for the possibility of movement of the C—S—H layers bounding the space, the results are not directly comparable with experimental data and, hence, are not shown in Fig. 3.

The different methods of obtaining the interlayer water content on desorption are in reasonable agreement: atomistic predictions, NMR measurements, and the simple approximation of linear desorption [see Fig. 3(c)]. Water at a given RH on adsorption from the dry state is always less than that present at the same RH on desorption. Figure 3(d) shows the comparison between the original sorption isotherm and the reduced isotherm obtained by subtracting the estimated interlayer water content on both desorption and adsorption. The bump at small RH in the reduced isotherm is due to the oversimplifying assumption of linear desorption from the interlayer space. In fact, molecular simulations indicate that a variety of interlayer widths [see Figs. 2(c) and 3(c)] will suffice to justify a shape of the interlayer desorption that is more complex than our simple linear assumption. This aspect can be refined in the future, but we regard our first approximation as a satisfactory starting point.

## 2. Gel and capillary pore water

Having subtracted the interlayer water, the resulting reduced isotherm in Fig. 3(d) is assumed to reflect only water located in the gel and capillary pores. A description of sorption in the gel and capillary pores must contain two fundamental ingredients: a model relating water content to pore width and an explanation of the hysteresis mechanism. We follow the precedent of widely used continuum models of water sorption in mesoporous materials, such as the Barrett-Joyner-Halenda (BJH) theory [40] and combine

adsorption on the pore surfaces with the Kelvin equation for capillary condensation.

The Kelvin equation [40] allows the calculation of the radius of curvature of a liquid-vapor interface in equilibrium with a particular RH. This radius of curvature can be used as a measure of pore width, although assumptions about the pore and meniscus shape and the contact angle between the condensed water and the pore wall must be made in order to calculate a specific quantity such as pore radius. Since the important ingredient of our model is a general division of the water according to its location rather than a precise knowledge of pore size, we make the simple assumption of cylindrical pores, with zero contact angle due to the adsorbed layer. The equilibrium phase transition in a pore of diameter  $d$  then takes place when

$$\ln(h) = -\frac{4\gamma_w a^3}{(d - 2a\theta)kT}, \quad (1)$$

where  $h$  is the RH,  $\gamma_w$  is the surface tension of water (72 mN m<sup>-1</sup> at room temperature),  $a^3$  is the characteristic volume of a water molecule in the liquid state (0.030 nm<sup>3</sup>),  $\theta_a$  is the thickness of the adsorbed layer (see below),  $k$  is the Boltzmann constant, and  $T$  is absolute temperature (298 K). The volume of pores of a particular width can be found by differentiating the sorbed mass with respect to width.

There are two main sources of hysteresis in sorption in the gel and capillary pores. The first arises in single pores, where a difference in the shape of the meniscus during the filling and emptying processes results in these processes occurring at different RH. We account for this hysteresis with the simple assumption that (in the absence of network effects described below) pores empty at equilibrium but fill at the equilibrium emptying RH of pores twice their diameter. This assumption is chosen, as it is true for idealized open-ended cylindrical pores [41], but we are not claiming literal cylindrical pores; we are simply choosing an approximation that is midway between maximum single-pore hysteresis (as for slit pores) and perfect equilibrium on filling.

The second source of hysteresis is a phenomenon known as pore blocking, sometimes called the “ink-bottle” effect [42,43]. This is when, during desorption, the presence of many full pores restricts the access of some pores to a liquid-vapor interface, preventing them from emptying at the equilibrium RH value associated with their size. Numerous models of pore blocking have been developed [19,27,42,44–46]; the appropriate choice of model depends on the structure of the porous material. We use a simple percolation model [47] of pore blocking to predict the condensed water content during desorption. The distinct knee around 40% RH in the desorption isotherm arises because at such low RH the pores start to empty even if not in contact with the vapor phase. A previous study [19] used a very similar approach but applied a pore-blocking model

not only to the gel pores but also to the interlayer space. We believe that pore blocking does not influence the removal of water from the interlayer space, as this space is surrounded by gel pores, which will already be empty at the RH at which the interlayer space begins to empty. Hysteresis in the interlayer space can, instead, arise from single-pore effects due to the molecular nature of water [48,49], strong electrostatic interactions among dissolved ions and the C–S–H surface [21,50], and the collapse of the space.

### 3. Surface-adsorbed water

In addition to condensed water in the pores, there will be adsorbed water on the pore surfaces. The volume of this water is calculated by multiplying the surface area of empty pores (as given by the pore-width distribution) by the fractional surface coverage and the thickness of a monolayer. To calculate the surface coverage, we use the Langmuir equation [51]

$$\theta = \frac{ah}{1 + ah}, \quad (2)$$

where  $\theta$  is the coverage as a fraction of a full monolayer, and  $a$  is a constant related to the energy of adsorption. In Appendix B we show that using the Brunauer-Emmett-Teller (BET) equation instead of the Langmuir equation [Eq. (2)] leads to very similar results. We assume  $a = 65$ , which in the BET approach corresponds to the presence of a single monolayer of pore surface-adsorbed water at RH of 11%, as generally accepted [37,38]. The calculation of the pore-width distribution and the adsorbed water content on the surface is performed iteratively.

## B. Results

Figures 4(a)–4(c) show the individual contributions of interlayer, pore (gel and capillary), and surface-adsorbed water to the sorption isotherm. The greatest fraction of water is located in the pores, though the interlayer water content is also significant. The quantity of water adsorbed on pore surfaces reaches a maximum at relatively low RH: as RH is further increased, this water is not removed but is reclassified as gel pore water once the pores in which it is adsorbed fill up. This reclassification has been noted experimentally in NMR measurements of the water content of different pore types [31]. This reclassification also causes the hysteresis in the quantity of surface water, as more pores are full on drying than on wetting. Figure 4(d) compares the modeled sorption isotherm obtained by summing the individual contributions plotted on the left to the experimental isotherm of Feldman and Sereda [27]. The model captures the general shape of the sorption hysteresis. There is some discrepancy at very low RH on drying, which we attribute to the oversimplification in the computation of interlayer water content.

Figure 5 shows the pore-width distribution found by differentiating the pore water content on adsorption [27] with respect to pore width. The range of pore widths that can be assessed is limited at the lower end by overlap with the effect of the interlayer space and at the upper end by the loss of resolution as the RH approaches 100% (for example, 98% RH corresponds to a Kelvin radius of 50 nm and 99% to a radius of 100 nm). The distribution has a peak around 2 nm and a very wide tail extending at least to many tens of nanometers. A logarithmic  $x$  axis makes it clear that a substantial fraction of the porosity comes from large

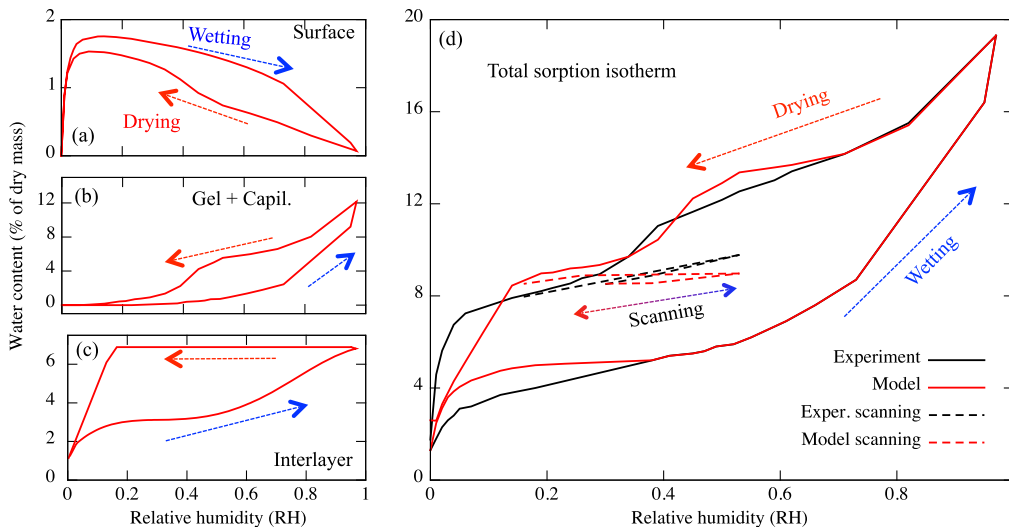


FIG. 4. Model for the water sorption isotherm. The contributions to the sorption isotherm from water (a) adsorbed on pore walls, (b) present in filled gel and capillary pores (the gel pore water content during wetting is taken from experiment, while that during drying comes from a chain model of pore blocking) and (c) present in the interlayer space. (d) Final model result (red) obtained by summing the three curves on the left, along with the experimental isotherm (black) for bottle-hydrated portland cement [27].

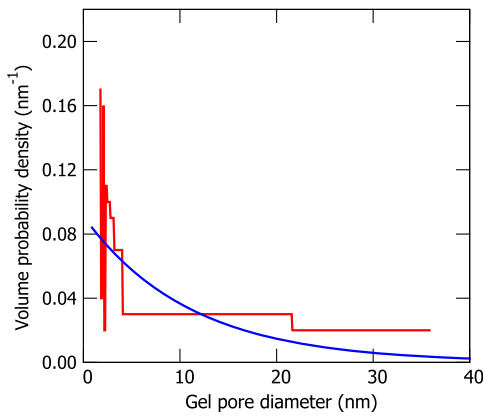


FIG. 5. Estimated pore-width distribution. The red line is obtained by differentiating the experimental gel pore water content [27] with respect to pore width. The blue line is an exponential fit used exclusively to calculate the surface-adsorbed water (Sec. III A 3), where using directly the data in red would have produced significant irregularities in the sorption curves.

pores. Similar pore distributions were obtained by Baroghel-Bouny [18] by applying the BJH theory to the desorption isotherm (an even greater contribution from large pores would have emerged if they had applied the BJH theory to the adsorption isotherm, which we argue is more correct).

#### IV. CONTINUUM MODELING OF REVERSIBLE DRYING SHRINKAGE

We now demonstrate the utility of the division of water into categories by presenting a model of reversible drying shrinkage. Reversible as a descriptor of drying shrinkage means that a bulk sample returns to its original dimensions when fully resaturated: there is still extensive hysteresis in the strain at intermediate RH values. Irreversible drying shrinkage, when the sample does not return to its original dimensions on resaturation, is observed primarily on the first cycle of drying and rewetting; the mechanisms for this irreversible shrinkage can involve plastic microstructural deformations and viscous effects (creep) and are not part of the models discussed here. We assume throughout that shrinkage is isotropic, so the linear strain measured in experiment is one-third of the volumetric strain.

Several continuum models of deformations induced by RH changes have been proposed [1–3]. Typically, these models are based on poromechanics and relate the volumetric strain to the Laplace pressure generated by liquid-vapor interfaces in the pore system (also known as capillary stress) [30,52,53]. Recent models have also provided a microporomechanical framework that accounts explicitly and separately for the pressure in macropores, mesopores (1–50 nm wide), and micropores (< 1 nm wide) [54]. Here we associate these contributions with the three categories of water already used to model the sorption isotherm (gel and capillary pore water, surface-adsorbed water, and interlayer

water). Because of the small linear strain during shrinkage (here, below 0.5%), we assume linear constitutive equations, and, therefore, we decompose the total strain into the sum of three contributions that can be treated independently from each other (under the further assumption of zero external stress):  $\epsilon_L$  from Laplace pressure in the gel and capillary pores,  $\epsilon_S$  from surface energy, and  $\epsilon_I$  from interlayer water. The low strain magnitude also means that the gel and capillary pore width can be approximated as fixed. We neglect the effect of any gradient in saturation, as this gradient will be small when the RH is changed in steps and the system is allowed to equilibrate.

To explain observed shrinkage in this way, it is necessary to be convinced that the hysteresis due to creep is unimportant, at least after any irreversible processes occurring on first drying. Strong evidence that hysteresis due to creep is unimportant in very mature pastes can be found in the work of Hansen [55]. Figure 2 of the cited paper shows that shrinkage is described by a single function of water content even though the time taken to reach this water content differs by up to 3 orders of magnitude. The accuracy of such a description implies that the hysteresis in strain is mostly a reflection of the sorption hysteresis, not a delayed response from the material.

This interpretation is consistent with experimental results for scanning isotherms on adsorption [56], which also find that shrinkage is a function of water content when scanning loops are small enough to provide little sorption hysteresis, and with observations that volumetric creep induced by external pressure significantly tapers off after 10–20 days (e.g., Refs. [57,58]). Similar behavior has also been observed in clay minerals (e.g., Refs. [26,59]).

To achieve this dependence of shrinkage on water content alone, it is necessary to equilibrate the sample sufficiently: 10–20 days is typical. On shorter time scales, time dependence can be observed, but Hansen’s results [55] indicate that this time dependence is due to the transient movement of water in the pores and is not inconsistent with a unique relationship between water content and length locally.

A time-independent approach is even sufficient to describe shrinkage in the very low RH region (see below, particularly, the contribution from interlayer water). However, this region displays large hysteresis in both water content and shrinkage, and due to the size of this hysteresis and the difficulty of accurately determining the interlayer water content, the presence or absence of creep effects cannot be definitively established.

Based on the above considerations, our model of shrinkage described below neglects time-dependent behaviors. Nevertheless, since our model can be seen as a particular solution of the general poromechanics problem in Ref. [54], further complexity and viscous effects can, in principle, be added in the future (e.g., following Refs. [30,60]). The advantage of our simplified approach is that it leads to essential expressions that highlight clearly the contribution

from the underlying physical mechanisms controlling shrinkage in relation to the water content, viz., to the sorption isotherms discussed previously.

### A. Macroscopic length change due to Laplace pressure

A simple and widely used constitutive model describing the strain of an isotropic porous material due to Laplace pressure in the gel pore water is [2,23,30,61]

$$\varepsilon_L = \frac{1}{3} \frac{kT}{a^3} \ln(h) S \left[ \frac{1}{K_b} - \frac{1}{K_s} \right]. \quad (3)$$

Here,  $kT \ln(h)/a^3$  is the Laplace pressure in the pore water,  $K_b = 19$  GPa is the bulk modulus of the macroscopic sample,  $K_s = 50$  GPa is the bulk modulus of the solid part of the C–S–H gel [62], and  $S$  is the filling fraction of the gel and capillary pores. Equation (3) is a well-known expression in the field of poromechanics, and the general framework from which it derives can incorporate time-dependent and multiphysics processes not considered here (e.g., Refs. [30,60]).

### B. Macroscopic length change due to surface energy

The Bangham equation [55,63,64] describes the shrinkage due to the change in surface tension resulting from the dependence of adsorbed layer thickness on RH. We treat the system at 100% RH, when all solid surfaces are covered by water and there is little or no liquid-vapor interface area, as the reference state and calculate surface tension and shrinkage relative to this case. The surface tension at the wall of a pore that remains full will be almost constant, so we modify the Bangham equation such that the length change depends only on the area uncovered as pores empty (note that “empty” pores remain lined by a layer of surface-adsorbed water). The linear strain due to surface energy is then

$$\varepsilon_S = -\frac{\Delta(\sigma\gamma)}{3K(1-2\nu)}, \quad (4)$$

where  $\sigma$  is the surface area of empty pores per volume of porous material,  $\gamma$  is the additional surface tension of the pore wall with its adsorbed layer relative to the surface tension of a pore wall adjacent to a full pore, and  $\nu$  is Poisson’s ratio of the bulk macroscopic volume, approximately 0.2 (see, e.g., Ref. [65]). At 100% RH, all pores are full, with the possible exception of some very large pores with low surface area, so  $\Delta(\sigma\gamma) = \sigma\gamma$ .

The surface tension is given by the Gibbs equation [64,66]:

$$\gamma = \gamma_0 - \frac{kT}{a^2} \int_{h_0}^h \theta \frac{dh}{h}, \quad (5)$$

where  $\gamma_0$  is the surface tension at  $h_0$ . We use saturation 100% RH as the reference RH. We assume that at 100% RH, we can neglect any interaction between the solid-fluid and fluid-vapor interfaces. Thus, the additional surface tension of this configuration relative to that of the wall of a full pore is

simply the surface tension of the interface between the adsorbed fluid and vapor, which we assume to be that of bulk liquid, i.e.,  $\gamma_0 = \gamma_w$ .

### C. Macroscopic length change due to loss of interlayer water

It is well established that many layered materials experience expansion when a substance is intercalated into them [67–70], but the details of this expansion can be complex. An accurate model of the relationship between the quantity of interlayer water in C–S–H and the associated length change of the macroscopic cement paste sample will be rather difficult to develop. The presence of dissolved ions produces a repulsive osmotic pressure, but this is small: a mean field treatment with walls separated by 0.5 nm gives a pressure around 1 MPa or less, regardless of ion concentration [71]. More important than osmotic pressure are effects arising due to the discreteness of ions: correlation effects can even result in a force that is joining instead of disjoining [53,72].

GCMC simulations (see Appendix C) find that the separation of C–S–H layers decreases by approximately 17% on drying from 100% to 0% RH. This result agrees with x-ray diffraction experiments, which indicate 20% shrinkage at this scale [73]. In the same set of experiments, the macroscopic shrinkage of a bulk C–S–H sample is approximately 3% [73]. This implies that the heterogeneous structure of cement paste is capable of taking up most of the microscopic length change, and only a small fraction is transmitted to overall strain. A digital-image-based deformation mapping technique applied to the drying of cement paste [74] has shown an even larger ratio of local to bulk strain: local deformation of up to 50% for an overall strain of less than 0.5%.

In the absence of a detailed model that accurately captures both the local and macroscopic effects, we can make useful progress with the simple assumptions that the strain of the bulk cement paste is isotropic and is linearly proportional to the quantity of interlayer water, such that

$$\varepsilon_I = \frac{\lambda}{3} v_I, \quad (6)$$

where  $v_I$  is the volume of interlayer water (which can be calculated using the method described in the previous section; see Fig. 4), and  $\lambda$  is a proportionality constant. Although  $\lambda$  is found empirically in this work and, thus, may be considered a fitting parameter, it accounts for two possible and physically relevant phenomena: (1) that only part of the microscopic strain is accommodated by the porous material and (2) that only some of the interlayer spaces undergo swelling when water is intercalated into them, while the others do not undergo dimensional changes. [Assuming this mechanism for coal, Brochard *et al.* [75] obtained an expression equivalent to Eq. (6). Furthermore, the existence of interlayer spaces in cement

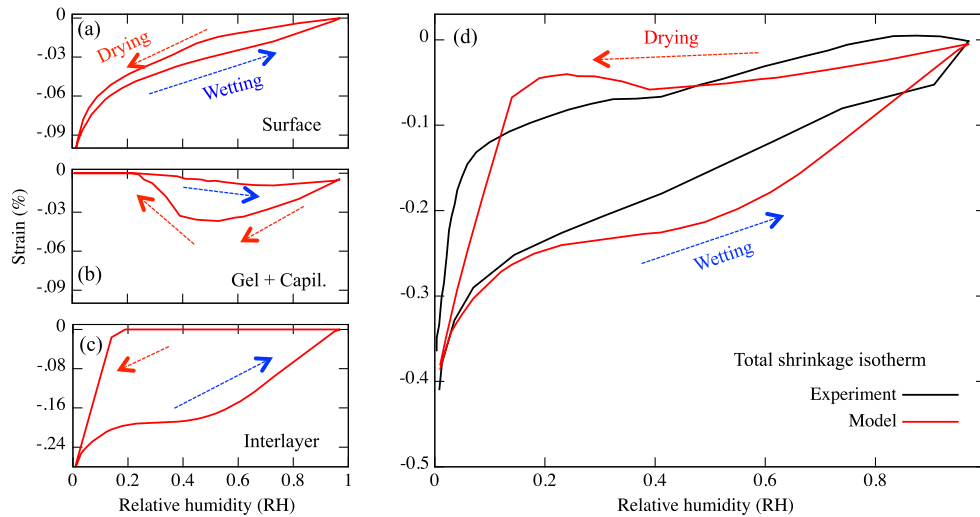


FIG. 6. Shrinkage associated with the sorption isotherms in Fig. 4. Our model’s prediction of the contributions from water (a) on the surface of C–S–H, (b) in the gel pores, and (c) in the interlayer spaces. (d) Sum of our model’s contributions from the left panels (red) and experiment (black) [27]. The saturated state is taken as reference by defining linear strain of 0 at RH of 1.

paste with different swelling behaviors was postulated in Ref. [17], where the nonswelling spaces were named “intragranular pores (IGP)”. Both of the phenomena discussed above entail strain localization, and the value of  $\lambda$  calculated here can potentially be used to assess models linking microscopic and macroscopic strains in cement paste. Experiments showing roughly a factor of 10 difference between these strains [73,74] suggest that we should expect  $\lambda \approx 0.1$ .

#### D. Comparison with experiment

Figures 6(a)–6(c) show the individual drying strain contributions from surface-adsorbed, pore (gel and capillary), and interlayer water predicted by our model. Figure 6(d) shows the overall predicted shrinkage (red line) along with the experimental data of Feldman and Sereda [27] (black line). In the experiment, the sample is dried by degassing at 80 °C, a very severe drying method which is expected to produce a significant hysteresis in water content and, consequently, in shrinkage strain at low relative humidity (cf. the less severe drying methods used in Refs. [18,36], respectively, 2% RH and approximately  $10^{-7}$  RH). The unknown parameter  $\lambda$  from Eq. (6) is used as the only fitting parameter; the best-fit value obtained is  $\lambda = 0.07$ , which is substantially smaller than 1, as expected (see Appendix D for further discussion of the effect of  $\lambda$ ). The combined model successfully reproduces the magnitude and general shape of the hysteresis in the reversible drying strain across the entire RH range.

The model explains the source of the observed shrinkage and its hysteresis. There is little hysteresis in the shrinkage caused by surface tension; this is a consequence of the negligible role played by the time-dependent behavior and of the small hysteresis in surface water content predicted by our

model in Sec. III. The hysteresis in the shrinkage caused by Laplace pressure is in the opposite direction to the overall shrinkage hysteresis (see Fig. 6). Only by accounting for the swelling effect of interlayer water can the observed hysteresis in the shrinkage be understood. For this reason, models based exclusively on Laplace pressure are unable to explain the experimental results. The importance of interlayer water also means that we can predict that if a sample is not dried below 15%–25% RH, much of the shrinkage hysteresis will disappear, and the remaining hysteresis will be in the opposite direction; that is, shrinkage as a function of RH will be greater during desorption than adsorption as with many other porous materials such as Vycor. This hypothesis is partly confirmed by Feldman and Sereda [66], who observed that the inverse behavior disappears when rewetting is started before drying below 25% RH.

The largest discrepancy between the mesoscale model prediction and experimental data in Fig. 6(d) is that the model predicts a transitory swelling upon drying between about 30% and 20% RH, but this relaxation is not observed in the experiment. The absence of relaxation suggests that the smallest gel pores empty more gradually than is predicted by the sorption model. Shrinkage modeling can be improved through the use of NMR coupled with length-change measurements, as well as by molecular-scale simulations that allow pore-wall displacement and consideration of electrolyte effects. Nevertheless, our current ability to predict the general shape of the length-change isotherm shows the benefit of dividing the pores by type and considering separately the water in each type of space.

#### V. DISCUSSION

The importance of porosity in determining the compressive strength of cement paste has been known since Powers

and Brownyard [44] first defined capillary pores. However, the evaluation of the relationship between microstructure and other properties, such as drying shrinkage and creep behavior, remains mostly qualitative. The main observation of this work is that classifying the water in cement paste according to its location—in interlayer space, in pore space, or adsorbed on surfaces—and then modeling the physical behavior of each of these water types separately, allows the overall behavior of the paste to be better understood.

For instance, gel water is almost completely evaporated at 15%–25% RH, while the interlayer water has generally not begun to evaporate. Subtracting interlayer water, as broadly defined here, from the total water content allows the calculation of the water content of the gel pores. This then allows the pore-width distribution to be determined. A model based on one fitting parameter, which gives some information about the prevalence of capillary pores [47], accurately explains the hysteresis in the sorption isotherm.

We show how the division of water into categories allows the prediction of macroscopic engineering-scale drying shrinkage by identifying the pores responsible within any RH range. Previous work [17] has interpreted scanning adsorption isotherms to deduce the interlayer water content as a function of RH, but here it is extended to show that this water can induce a shrinkage hysteresis that is opposite to materials that do not intercalate water molecules into the solid molecular network, such as porous borosilicate glass. The hysteresis caused by the interlayer water largely disappears if a sample is not dried below 25% RH [66].

The understanding of the fundamental importance of the difference between water in different locations and of the different RH ranges over which these locations empty and fill, opens the door to a new perspective for designing experiments that extract information about the microstructure of cement-based materials. For example, the gel pores can be probed without interference from interlayer space by drying only to about 25% RH. The size distribution of the gel pores can then be analyzed from the adsorption isotherm and their connectivity to the larger pores by analysis of the hysteresis. Such analysis can be used, for example, to assess the gel-pore ratio and initial water-to-cement ratio of an existing sample of cement. The structure of gel pores can change due to drying, load, or even deliberate alteration such as by filling these (10–100)-nm-scale spaces with polymer [76]. Since such a change in structure will greatly influence properties, our proposed technique for assessing the gel pore structure can be a valuable research tool. In addition, it can complement and support the validation of a growing body of mesoscale coarse-grained simulations aimed at elucidating the mechanisms of formation, the nanoscale structure, and the mechanical properties of the C–S–H gel [77–84]. There is also much scope for interesting research on the kinetics of water leaving each kind of space, which we do not treat here.

## VI. CONCLUSIONS

A physical model that captures the water sorption isotherm of cement paste, including its hysteresis, is presented and then used to obtain parameters for a model of reversible drying shrinkage, including its hysteresis, during drying and rewetting. We consider only sorption and strain after a full first drying-wetting cycle, which is a rare scenario in real engineering applications. Nevertheless, our gained understanding of the reversible sorption and shrinkage provides the necessary starting point to include further mechanisms of irreversible microstructural changes. Our proposed mesoscale models for sorption and for shrinkage supported by molecular-scale simulations and experiments decouple the water in the interlayer space from water in the somewhat larger gel and much larger capillary pores. Upon drying, water does not leave the interlayer space until 15%–25% RH, but during rewetting, it reenters the interlayer space over almost the entire RH range. The models are based on simple thermodynamic principles and supported by both molecular-scale models and experiments. The water in the interlayer space has a swelling effect, which is the source of the shrinkage hysteresis in the opposite direction to that of continuous materials such as porous borosilicate glass. This opposite behavior observed in cement paste is similar to natural materials such as clay. The overall model has just two empirical parameters that must be calculated from experimental data and correspond to important properties of the cement paste: the connectedness of the gel pore network to larger empty pores and the extent to which local volume changes cause overall volume changes of the macroscopic sample. Moreover, the construction of this physical continuum model informed by molecular and mesoscale simulations highlights new opportunities and questions for computational modeling of this complex material's physical properties.

## ACKNOWLEDGMENTS

We gratefully acknowledge the financial support of Portland Cement Association and the Ready Mixed Concrete Research and Education Foundation (supporting the MIT Concrete Sustainability Hub) and Schlumberger. H. M. acknowledges the Juan de la Cierva fellowship from the Spanish Ministerio de Industria y Competitividad and the financial support from the Basque Country Government Etorrek 2014 project.

## APPENDIX A: EQUATIONS OF THE SORPTION MODEL

In our sorption model, the first step towards calculation of the sorbed mass during wetting is to use Eq. (1) to calculate the radius of mean curvature  $R$  that controls filling at a given RH and calculate the surface layer thickness  $\theta$  using Eq. (2). The total adsorbed plus gel and capillary pore water mass is then

$$m_{\text{wet}} = \int_0^{R+2a\theta} v(l)\rho dl + Aa\theta\rho, \quad (\text{A1})$$

where

$$A = \int_{R+2a\theta}^{\infty} \frac{4v(l)}{l} dl \quad (\text{A2})$$

is the surface area of unfilled pores per unit volume.  $v(l)$  is the volume probability density of pores of width  $l$ ,  $\rho$  is the density of condensed water, and  $a$  is the thickness of a monolayer.

At the same RH on drying, the proportion of pores below their equilibrium emptying RH that do, in fact, empty is

$$Q = 1 - (1-f)(1-X)^4, \quad (\text{A3})$$

where

$$X = q[f + (1-f)(1 - (1-X)^3)], \quad (\text{A4})$$

and

$$q = \frac{\int_{2R+2a\theta}^{\infty} v(l)/l^2 dl}{\int_0^{\infty} v(l)/l^2 dl} \quad (\text{A5})$$

is the number fraction of pores larger than  $2R + 2a\theta$  and, hence, are able to empty if they have access to the liquid-vapor interface, and  $f$  is the fraction of pores initially exposed to this interface. The adsorbed plus gel and capillary water mass is then

$$m_{\text{dry}} = \int_0^{2R+2a\theta} v(l)\rho dl + (1-Q) \int_{2R+2a\theta}^{\infty} v(l)\rho dl + QAa\theta\rho. \quad (\text{A6})$$

## APPENDIX B: CHOICE OF ISOTHERM FOR SURFACE ADSORPTION

In the main text we calculate the quantity of water adsorbed on pore walls using the Langmuir equation. A popular alternative to this description is the BET equation [85],

$$\theta = \frac{ah}{[(\alpha-1)h+1](1-h)}. \quad (\text{B1})$$

Using this equation instead gives very similar results: Figs. 7 and 8 show the categorization of water into types and the predicted shrinkage using the BET equation for surface adsorption. The apparent hysteresis in the surface water content exists simply because water in full pores is always classified as condensed, not adsorbed. The quantity of surface-adsorbed water predicted by the BET model is qualitatively different from the Langmuir case in Fig. 4(a) because the BET equation predicts an indefinitely increasing thickness of the adsorbed layer as RH tends to 100%.

In this paper, we prefer the Langmuir model [Eq. (2)], as the distinction between adsorbed and condensed water is clearer. Of course, the ideal curve to use would be one obtained by the experimental measurement of the thickness of the adsorbed layer on a flat C—S—H surface as a function of RH if such a curve were available.

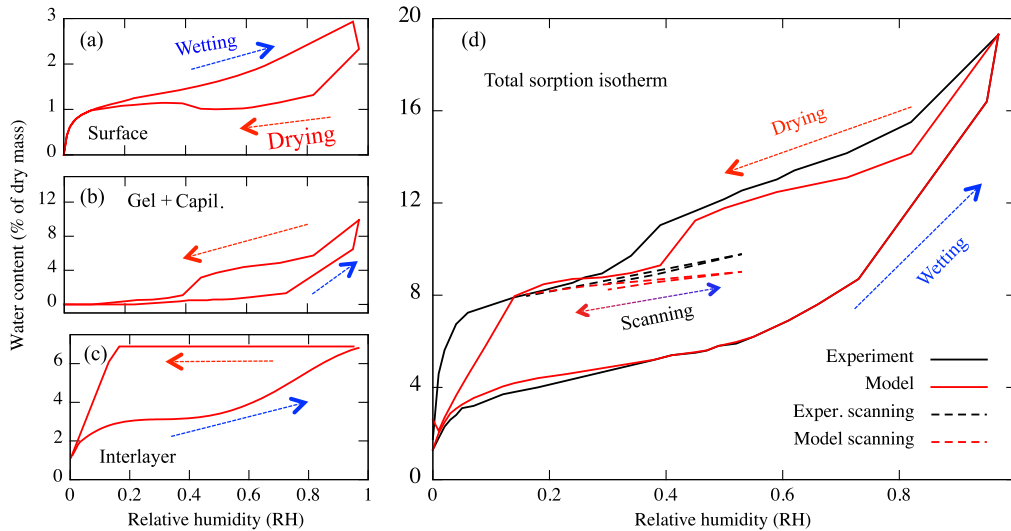


FIG. 7. Model for the water sorption isotherm using the BET equation for surface adsorption. The contributions to the sorption isotherm from water (a) adsorbed on pore walls, (b) present in filled gel and capillary pores and (c) present in the interlayer space. (d) Final model result (red) obtained by summing the three curves on the left, along with the experimental isotherm (black) for bottle-hydrated portland cement [27].

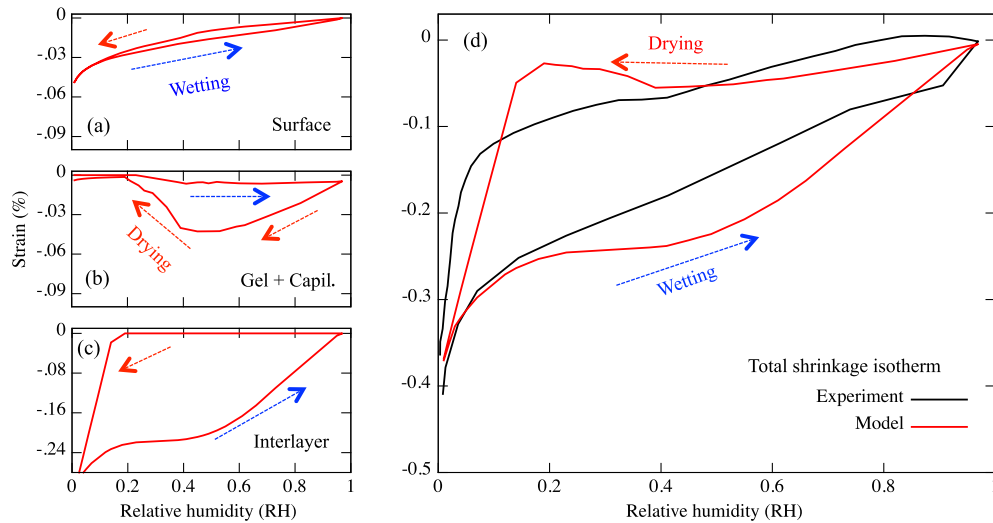


FIG. 8. Shrinkage associated with the sorption isotherms in Fig. 7. Our model's prediction of the contributions from water (a) on the surface of C—S—H, (b) in the gel pores, and (c) in the interlayer spaces. (d) Sum of our model's contributions from the left panels (red) and experiment (black). The saturated state is taken as reference by defining strain of 0 at a relative humidity of 1.

### APPENDIX C: VOLUMETRIC SHRINKAGE AND LINEAR DRYING STRAIN FROM MOLECULAR SIMULATIONS

Here we provide some additional details regarding the molecular simulations that we use to estimate the drying shrinkage of single C—S—H particles due to the loss of interlayer water. We combine GCMC and molecular dynamics (MD) to obtain iteratively the thermodynamically predicted amount of water and the corresponding volume of the C—S—H particle for a given relative humidity. The interactions between atoms of the molecular structure are computed using the CSH force field [86], combining a Lennard-Jones interaction potential for dispersion-repulsion interactions between atoms and partial charges carried by each atom of the molecular structure for electrostatic interactions. In GCMC simulations, the C—S—H molecular structure is in equilibrium with an infinite reservoir (the environment) that imposes its temperature and its chemical potential (or RH) [87]. In such simulations, equilibrium is achieved by randomly (Markov chain) inserting and removing water and by randomly moving atoms in the molecular structure. Acceptance of each insertion, deletion, and move is driven by a law proportional to the Boltzmann factor. By varying RH, we then get a different amount of water in the molecular structure allowing us to build adsorption and desorption isotherms. We use  $10^6$  steps to reach equilibrium for each simulation point at 300 K. For all considered RH, an energy minimization of the molecular structure with the conjugate gradient method is then performed. The equilibrated and energy-minimized structures are relaxed with a MD simulation in the isothermal-isobaric ensemble, where the molecular structure is now in equilibrium with a huge reservoir imposing its temperature and pressure. The volume of the molecular

structure is adjusted with respect to the two latter thermodynamics quantities. We use a zero pressure to obtain the relaxation due solely to the temperature (finite-temperature entropic effects). The length of the MD run in the isothermal-isobaric ensemble is 50 ns with a time step of 0.1 fs. Finally, a MD simulation run of 20 ns in the canonical ensemble, where the reservoir is imposing only its temperature, with a time step of 2 fs is performed, and sampling of configurations is done over the last 10 ns every 1 ps. In the previously described simulations, we compute the volumetric shrinkage of a single C—S—H particle by monitoring the volume of the molecular structure and the linear drying strain in the direction normal to the C—S—H layers by monitoring the basal length change when the cement paste is dried to 0% RH and after volume relaxation. After complete drying, we compute a volumetric shrinkage of approximately 17% and a linear drying strain of approximately 12% corresponding to a basal spacing of 0.94 nm (i.e., the distance between two silicate-rich layers surrounding a water-rich layer of the C—S—H unit cell). The volumetric shrinkage computed by these simulations is on the same order of magnitude as that measured for a dried cement paste reported as 50% deformation [74]. The linear drying strain is also in reasonably good agreement with that reported in drying experiments, 20% [73]. We note that both the linear and volumetric measures of dimensional changes in C—S—H particles are currently overestimated by these simulations, as compared with those inferred from experiments. The discrepancy between basal spacing predicted by our simulations (0.94 nm) and that measured experimentally (1.13 nm [73]) indicates that the simulations can be improved to quantitatively predict shrinkage of C—S—H particles, as well as the multiparticle C—S—H aggregates described as a C—S—H gel [22].

#### APPENDIX D: ASSUMPTION OF LINEAR SWELLING DUE TO INTERLAYER WATER

Our model for bulk shrinkage assumes that the length change due to interlayer water is linearly dependent on the interlayer water content: the constant of proportionality  $\lambda$  is a free parameter calculated by comparison with experimental results. Since this assumption is an important part of the shrinkage model, here we compare it with alternate assumptions. We identify four competing assumptions.

- (1) Interlayer water has no influence on shrinkage ( $\lambda = 0$ ), e.g., if all interlayer water is located in small pores that do not collapse on water removal.
- (2) Expansion is, indeed, proportional to water content but with a much higher proportionality constant ( $\lambda = 1$ ), assuming that water insertion causes swelling of the solid by the entire volume of the water, and this expansion is, in turn, entirely passed on to the macroscopic length.
- (3) Expansion is not linear, but the first water inserted causes the bulk of expansion, while the water inserted at the highest RH causes little expansion, as it is entering layers that have already been separated. We model the origin of these pores using a parabolic dependence of expansion on interlayer water content, with zero slope at complete filling.
- (4) Swelling is, indeed, directly proportional to water content but acts in the gel pores just as much as the interlayer space [i.e.,  $v_I$  in Eq. (6) becomes the volume of water in gel and capillary pores plus interlayer spaces instead of interlayer water only).

The predictions made using these four distinct assumptions are shown in Fig. 9.

The first and second assumptions lead to predicted shrinkages that are quantitatively not comparable with the experimental measurements (see Fig. 9). By contrast, both the assumption of linear shrinkage that we use in the

main body of the paper and the third assumption presented here (quadratic length change) give good agreement between model and experiment. The fourth assumption leads to a reasonable quantitative agreement with the experiment, but the predicted shape of the hysteresis differs significantly from the experiment. All of this suggests that it is, indeed, only water in the interlayer space that is causing expansion and that it must be of the magnitude assumed here, but the details of the relationship between water content and strain (e.g., linear or parabolic) remain unknown.

To gain a more precise understanding of the mechanisms of swelling of interlayer water, it is necessary to turn to molecular models that can probe the dominant forces. In these spaces, water is confined strongly, so a continuum treatment is not valid. Molecular dynamics simulations [21,22,50,88,89] have shown that water in the interlayer space can exhibit density considerably higher than that of bulk water. As discussed in the main text, GCMC simulations are able to calculate the interlayer water content on desorption [21], giving values that agree with NMR experiments. An accurate model of sorption in the interlayer space will, thus, allow for pore walls that can displace as a function of water or electrolyte content, in response to forces from the adsorbed water and the surrounding solid. There is also direct confirming experimental evidence that has been obtained [32] showing the separation of layers as a function of RH. This evidence suggests that the collapse and reopening of the interlayer space provides an important contribution to sorption hysteresis in these spaces and represents an important future direction for GCMC simulations.

Additionally, molecular models can be used to calculate the pressure exerted by the fluid [21,72], which is dominated by strong electrostatic interactions among water molecules, dissolved ions, and the charged C—S—H

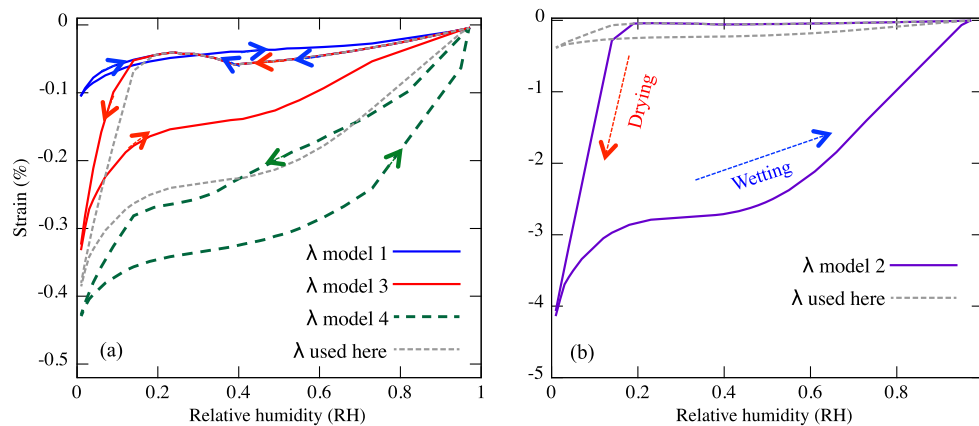


FIG. 9. (a) Predicted shrinkage using the value of  $\lambda$  given in the text, compared with the predictions of models based on alternate assumptions: model 1, no length change due to interlayer water, i.e.,  $\lambda = 0$ ; model 3, quadratic instead of linear length change; and model 4, swelling in the gel pores just as in the interlayer space. (b) Predicted shrinkage using the value of  $\lambda$  given in the text, compared with the prediction of model 2,  $\lambda = 1$ .

surfaces. For example, molecular models treating these effects have explained the observed hysteresis in the drying shrinkage of swelling clays, layered materials that share many features with cement paste [26,90,91]. The higher surface charge and disorder of cement paste make it a more challenging system to understand [53,92], but initial work [21] has been able to separate the important contributions to this fluid-induced or disjoining pressure, setting a promising ground for future studies. These positive pressures are fundamentally responsible for the opposite hysteresis of shrinkage compared to continuous materials such as porous glass. It is also important to understand the role of applied stress on shrinkage and, in particular, the role of applied stress on the interlayer water, which might shed light on the poorly understood Pickett effect [93].

- 
- [1] F. Benboudjema, F. Meftah, and J. M. Torrenti, Interaction between drying, shrinkage, creep and cracking phenomena in concrete, *Engineering structures* **27**, 239 (2005).
- [2] I. Vlahinić, H. M. Jennings, and J. J. Thomas, A constitutive model for drying of a partially saturated porous material, *Mech. Mater.* **41**, 319 (2009).
- [3] T. Rougelot, F. Skoczylas, and N. Burlion, Water desorption and shrinkage in mortars and cement pastes: Experimental study and poromechanical model, *Cement and Concrete Research* **39**, 36 (2009).
- [4] F. Wittmann, Einfluss des Feuchtigkeitsgehaltes auf das Kriechen des Zementsteines, Rheol, *Acta Academiae Aboensis Ser B, Mathematica et physica* **9**, 282 (1970).
- [5] F. H. Wittmann, Interaction of hardened cement paste and water, *J. Am. Ceram. Soc.* **56**, 409 (1973).
- [6] F. Wittmann, in *Cement and Production Use*, edited by Jan Skalny (Franklin Pierce College, Rindge, 1979), pp. 143–161.
- [7] Z. P. Bažant, F. C. Caner, I. Carol, M. D. Adley, and S. A. Akers, Microplane model M4 for concrete. I: Formulation with work-conjugate deviatoric stress, *J. Eng. Mech.* **126**, 944 (2000).
- [8] B. T. Tamtsia and J. J. Beaudoin, Basic creep of hardened cement paste: A re-examination of the role of water, *Cement and Concrete Research* **30**, 1465 (2000).
- [9] Z. P. Bažant, in *Encyclopedia of Material: Science and Technology*, edited by B. Ilshner (Elsevier, New York, 2001).
- [10] Z. P. Bažant, G. Cusatis, and L. Cedolin, Temperature effect on concrete creep modeled by microprestress-solidification theory, *J. Eng. Mech.* **130**, 691 (2004).
- [11] H. M. Jennings, J. W. Bullard, J. J. Thomas, J. E. Andrade, J. J. Chen, and G. W. Scherer, Characterization and modeling of pores and surfaces in cement paste: Correlations to processing and properties, *J. Adv. Concr. Technol.* **6**, 5 (2008).
- [12] H. F. W. Taylor, Proposed structure for calcium silicate hydrate gel, *J. Am. Ceram. Soc.* **69**, 464 (1986).
- [13] H. F. W. Taylor, *Cement Chemistry*, 2nd ed. (Thomas Telford, London, 1997).
- [14] I. G. Richardson, Tobermorite/jennite- and tobermorite/calcium hydroxide-based models for the structure of C–S–H: Applicability to hardened pastes of tricalcium silicate,  $\beta$ -dicalcium silicate, portland cement, and blends of portland cement with blast-furnace slag, metakaolin, or silica fume, *Cement and Concrete Research* **34**, 1733 (2004).
- [15] R. J.-M. Pellenq, A. Kushima, R. Shahsavari, K. J. Van Vliet, M. J. Buehler, S. Yip, and F.-J. Ulm, A realistic molecular model of cement hydrates, *Proc. Natl. Acad. Sci. U.S.A.* **106**, 16102 (2009).
- [16] K. Van Vliet, R. J.-M. Pellenq, M. J. Buehler, J. C. Grossman, H. M. Jennings, F. J. Ulm, and S. Yip, Set in stone? A perspective on the concrete sustainability challenge, *MRS Bull.* **37**, 395 (2012).
- [17] H. M. Jennings, Refinements to colloid model of C–S–H in cement: CM-II, *Cement and Concrete Research* **38**, 275 (2008).
- [18] V. Baroghel-Bouny, Water vapour sorption experiments on hardened cementitious materials part I: Essential tool for analysis of hygral behaviour and its relation to pore structure, *Cement and Concrete Research* **37**, 414 (2007).
- [19] H. Ranaivomanana, J. Verdier, A. Sellier, and X. Bourbon, Toward a better comprehension and modeling of hysteresis cycles in the water sorption–desorption process for cement based materials, *Cement and Concrete Research* **41**, 817 (2011).
- [20] E. J. Garboczi and D. P. Bentz, Computer simulation of the diffusivity of cement-based materials, *J. Mater. Sci.* **27**, 2083 (1992).
- [21] P. A. Bonnaud, Q. Ji, B. Coasne, R. J.-M. Pellenq, and K. J. Van Vliet, Thermodynamics of water confined in porous calcium-silicate-hydrates, *Langmuir* **28**, 11422 (2012).
- [22] P. A. Bonnaud, Q. Ji, and K. J. Van Vliet, Effects of elevated temperature on the structure and properties of calcium-silicate-hydrate gels: The role of confined water, *Soft Matter* **9**, 6418 (2013).
- [23] D. P. Bentz, E. J. Garboczi, and D. A. Quenard, Modelling drying shrinkage in reconstructed porous materials: Application to porous Vycor glass, *Model. Simul. Mater. Sci. Eng.* **6**, 211 (1998).
- [24] P. I. Ravikovitch and A. V. Neimark, Density functional theory model of adsorption deformation, *Langmuir* **22**, 10864 (2006).
- [25] R. J.-M. Pellenq, J. M. Caillol, and A. Delville, Electrostatic attraction between two charged surfaces: A (N, V, T) Monte Carlo simulation, *J. Phys. Chem. B* **101**, 8584 (1997).
- [26] B. Carrier, L. Wang, M. Vandamme, R. J.-M. Pellenq, M. Bornert, A. Tanguy, and H. Van Damme, ESEM study of the humidity-induced swelling of clay film, *Langmuir* **29**, 12823 (2013).
- [27] R. F. Feldman and P. J. Sereda, A model for hydrated portland cement paste as deduced from sorption-length change and mechanical properties, *Materiale de constructii : organ al Ministerului Industrializarii Lemnului si Materialelor de Constructii* **1**, 509 (1968).
- [28] J. M. Cases, I. Berend, M. Francois, J. P. Uriot, L. J. Michot, and F. Thomas, Mechanism of adsorption and desorption of water vapor by homoionic montmorillonite; 3, The  $Mg^{2+}$ ,

- Ca<sup>2+</sup>, and Ba<sup>3+</sup> exchanged forms, *Clays Clay Miner.* **45**, 8 (1997).
- [29] R. S. Haines and R. McIntosh, Length changes of activated carbon rods caused by adsorption of vapors, *J. Chem. Phys.* **15**, 28 (1947).
- [30] D. Gawin, F. Pesavento, and B. A. Schrefler, Modelling creep and shrinkage of concrete by means of effective stresses, *Materiaux et constructions Materials and structures* **40**, 579 (2007).
- [31] A. C. A. Muller, K. L. Scrivener, A. M. Gajewicz, and P. J. McDonald, Use of bench-top NMR to measure the density, composition and desorption isotherm of C—S—H in cement paste, *Microporous Mesoporous Mater.* **178**, 99 (2013).
- [32] L. J. Parrott, The effect of moisture content upon the elasticity of hardened cement paste, *Magazine of concrete research* **25**, 17 (1973).
- [33] T. C. Powers, Structure and physical properties of hardened portland cement paste, *J. Am. Ceram. Soc.* **41**, 1 (1958).
- [34] H. M. Jennings, Colloid model of CSH and implications to the problem of creep and shrinkage, *Materiaux et constructions Materials and structures* **37**, 59 (2004).
- [35] Arnaud C. A. Muller, Karen L. Scrivener, Agata M. Gajewicz, and Peter J. McDonald, Densification of C—S—H measured by 1H NMR relaxometry, *J. Phys. Chem. C* **117**, 403 (2013).
- [36] R. F. Feldman, Helium flow characteristics of rewetted specimens of dried hydrated portland cement paste, *Cement and Concrete Research* **3**, 777 (1973).
- [37] J. Hagymassy, Jr., I. Odler, M. Yudenfreund, J. Skalny, and S. Brunauer, Pore structure analysis by water vapor adsorption. iii. Analysis of hydrated calcium silicates and portland cements, *J. Colloid Interface Sci.* **38**, 20 (1972).
- [38] I. Odler, I. Hagymassy, Jr., M. Yudenfreund, K. M. Hanna, and S. Brunauer, Pore structure analysis by water vapor adsorption. iv. Analysis of hydrated portland cement pastes of low porosity, *J. Colloid Interface Sci.* **38**, 265 (1972).
- [39] R. J.-M. Pellenq, B. Coasne, R. O. Denoyel, and O. Coussy, Simple phenomenological model for phase transitions in confined geometry. 2. Capillary condensation/evaporation in cylindrical mesopores, *Langmuir* **25**, 1393 (2009).
- [40] E. P. Barrett, L. G. Joyner, and P. P. Halenda, The determination of pore volume and area distributions in porous substances. I. Computations from nitrogen isotherms, *J. Am. Chem. Soc.* **73**, 373 (1951).
- [41] L. H. Cohan, Sorption hysteresis and the vapor pressure of concave surfaces, *J. Am. Chem. Soc.* **60**, 433 (1938).
- [42] G. Mason, The effect of pore space connectivity on the hysteresis of capillary condensation in adsorption—desorption isotherms, *J. Colloid Interface Sci.* **88**, 36 (1982).
- [43] F. Moro and H. Böhni, Ink-bottle effect in mercury intrusion porosimetry of cement-based materials, *J. Colloid Interface Sci.* **246**, 135 (2002).
- [44] T. C. Powers and T. L. Brownyard, in *ACI Journal Proceedings* (ACI, 1946), Vol. **43**.
- [45] R. M. Espinosa and L. Franke, Ink-bottle pore-method: Prediction of hygroscopic water content in hardened cement paste at variable climatic conditions, *Cement and Concrete Research* **36**, 1954 (2006).
- [46] B. Coasne, A. Galarneau, R. J.-M. Pellenq, and F. Di Renzo, Adsorption, intrusion and freezing in porous silica: The view from the nanoscale, *Chem. Soc. Rev.* **42**, 4141 (2013).
- [47] M. B. Pinson, H. M. Jennings, and M. Z. Bazant, Inferring pore size and network structure from sorption hysteresis, [arXiv:1402.3377v1](https://arxiv.org/abs/1402.3377v1).
- [48] Z. P. Bažant and M. Z. Bazant, Theory of sorption hysteresis in nanoporous solids: Part I Snap-through instabilities, *J. Mech. Phys. Solids* **60**, 1644 (2012).
- [49] M. Z. Bazant and Z. P. Bažant, Theory of sorption hysteresis in nanoporous solids: Part II Molecular condensation, *J. Mech. Phys. Solids* **60**, 1660 (2012).
- [50] H. Manzano, S. Moeini, F. Marinelli, A. C. T. van Duin, F. J. Ulm, and R. J.-M. Pellenq, Confined water dissociation in microporous defective silicates: Mechanism, dipole distribution, and impact on substrate properties, *J. Am. Chem. Soc.* **134**, 2208 (2012).
- [51] I. Langmuir, The adsorption of gases on plane surfaces of glass, mica and platinum, *J. Am. Chem. Soc.* **40**, 1361 (1917).
- [52] Z. P. Bažant, Thermodynamics of interacting continua with surfaces and creep analysis of concrete structures, *Nucl. Eng. Des.* **20**, 477 (1972).
- [53] R. J.-M. Pellenq, N. Lequeux, and H. van Damme, Engineering the bonding scheme in C—S—H: The ionic-covalent framework, *Cement and Concrete Research* **38**, 159 (2008).
- [54] M. Vandamme, P. Dangla, S. Nikoosokhan, and L. Brochard, *Nonlinear Elasticity and Hysteresis: Fluid-Solid Coupling in Porous Media* (Wiley, New York, 2015), Chap. 5.
- [55] W. Hansen, Drying shrinkage mechanisms in portland cement paste, *J. Am. Ceram. Soc.* **70**, 323 (1987).
- [56] R. F. Feldman, Sorption and length-change scanning isotherms of methanol and water on hydrated portland cement, in *Proceedings of the 5th international symposium on the Chemistry of Cement*, Tokyo, Part III, vol III, 53 (1968).
- [57] O. Bernard, F.-J. Ulm, and J. T. Germaine, Volume and deviator creep of calcium-leached cement-based materials, *Cement and Concrete Research* **33**, 1127 (2003).
- [58] Z. C. Grasley and D. A. Lange, The viscoelastic response of cement paste to three-dimensional loading, *Mech. Time-Depend. Mater.* **11**, 27 (2007).
- [59] G. Montes-H, J. Duplay, L. Martinez, Y. Geraud, and B. Rousset-Tournier, Influence of interlayer cations on the water sorption and swelling-shrinkage of mx80 bentonite, *Appl. Clay Sci.* **23**, 309 (2003).
- [60] C. T. Davie, C. J. Pearce, and N. Bićanić, A fully generalised, coupled, multi-phase, hygro-thermo-mechanical model for concrete, *Materiaux et constructions Materials and structures* **43**, 13 (2010).
- [61] R. W. Lewis and B. A. Schrefler, *The Finite Element Method in the Static and Dynamic Deformation and Consolidation of Porous Media* (John Wiley, New York, 1998).
- [62] H. Manzano, E. Masoero, I. Lopez-Arbeloa, and H. M. Jennings, Shear deformations in calcium silicate hydrates, *Soft Matter* **9**, 7333 (2013).
- [63] D. H. Bangham and R. I. Razouk, The wetting of charcoal and the nature of the adsorbed phase formed from saturated vapours, *Trans. Faraday Soc.* **33**, 1463 (1937).

- [64] V. S. Ramachandran, R. F. Feldman, and J. J. Beaudoin, *Concrete Science* (Heyden & Son Ltd., London, 1981), pp. 66–68.
- [65] J. Sanahuja, L. Dormieux, and G. Chanvillard, Modelling elasticity of a hydrating cement paste, *Cem. Concr. Soc.* **37**, 1427 (2007).
- [66] R. F. Feldman and P. J. Sereda, Sorption of water on compacts of bottle-hydrated cement. II. Thermodynamic considerations and theory of volume change, *J. Appl. Chem.* **14**, 93 (1964).
- [67] M. S. Dresselhaus and G. Dresselhaus, Intercalation compounds of graphite, *Adv. Phys.* **30**, 139 (1981).
- [68] J. R. Dahn, D. C. Dahn, and R. R. Haering, Elastic energy and staging in intercalation compounds, *Solid State Commun.* **42**, 179 (1982).
- [69] B. R. York and S. A. Solin, Effect of composition on charge exchange, lattice expansion, and staging in potassium-ammonia graphite intercalation compounds, *Phys. Rev. B* **31**, 8206 (1985).
- [70] S. Lee, H. Miyazaki, S. D. Mahanti, and S. A. Solin, Composition-Driven c-Axis Expansion of Intercalated Layered Solids: 1D Non-Vegard's-Law Behavior in a 2D Solid Solution, *Phys. Rev. Lett.* **62**, 3066 (1989).
- [71] D. Andelman, Electrostatic properties of membranes: The Poisson-Boltzmann theory, *Handb. Biol. Phys.* **1**, 603 (1995).
- [72] A. Gmira, M. Zabat, R. J.-M. Pellenq, and H. Damme, Microscopic physical basis of the poromechanical behavior of cement-based materials, *Materiaux et constructions Materials and structures* **37**, 3 (2004).
- [73] W. A. Gutteridge and L. J. Parrott, A study of the changes in weight, length and interplanar spacing induced by drying and rewetting synthetic CSH (I), *Cement and Concrete Research* **6**, 357 (1976).
- [74] C. M. Neubauer, E. J. Garboczi, and H. M. Jennings, The use of digital images to determine deformation throughout a microstructure Part I Deformation mapping technique, *J. Mater. Sci.* **35**, 5741 (2000).
- [75] L. Brochard, M. Vandamme, and R. J.-M. Pellenq, Poromechanics of microporous media, *J. Mech. Phys. Solids* **60**, 606 (2012).
- [76] F. Merlin, H. Lombois, S. Joly, N. Lequeux, J.-L. Halary, and H. Van Damme, Cement-polymer and clay-polymer nano- and meso-composites: Spotting the difference basis of a presentation given at materials discussion No. 5, 22–25 September 2002, Madrid, Spain, *J. Mater. Chem.* **12**, 3308 (2002).
- [77] R. González-Teresa, V. Morales-Florez, H. Manzano, and J. S. Dolado, Structural models of randomly packed Tobermorite-like spherical particles: A simple computational approach, *Materiale de constructii : organ al Ministerului Industrializarii Lemnului si Materialelor de Constructii* **60**, 7 (2010).
- [78] T. Mazumdar, S. Mazumder, and D. Sen, Temporal evolution of mesoscopic structure of some non-Euclidean systems using a Monte Carlo model, *Phys. Rev. B* **83**, 104302 (2011).
- [79] E. Masoero, E. Del Gado, R. J.-M. Pellenq, F.-J. Ulm, and S. Yip, Nanostructure and Nanomechanics of Cement: Polydisperse Colloidal Packing, *Phys. Rev. Lett.* **109**, 155503 (2012).
- [80] R. González-Teresa, J. S. Dolado, A. Ayuela, and J.-C. Gimel, Nanoscale texture development of C–S–H gel: A computational model for nucleation and growth, *Appl. Phys. Lett.* **103**, 234105 (2013).
- [81] E. Masoero, E. Del Gado, R. J.-M. Pellenq, S. Yip, and F.-J. Ulm, Nano-scale mechanics of colloidal C–S–H gels, *Soft Matter* **10**, 491 (2014).
- [82] K. Ioannidou, R. J.-M. Pellenq, and E. Del Gado, Controlling local packing and growth in calcium-silicate-hydrate gels, *Soft Matter* **10**, 1121 (2014).
- [83] M. A. Etzold, P. J. McDonald, and A. F. Routh, Growth of sheets in 3d confinements—a model for the C–S–H meso structure, *Cement and Concrete Research* **63**, 137 (2014).
- [84] E. Masoero, J. J. Thomas, and H. M. Jennings, A reaction zone hypothesis for the effects of particle size and water-to-cement ratio on the early hydration kinetics of  $C^3S$ , *J. Am. Ceram. Soc.* **97**, 967 (2014).
- [85] S. Brunauer, P. H. Emmett, and E. Teller, Adsorption of gases in multimolecular layers, *J. Am. Ceram. Soc.* **60**, 309 (1938).
- [86] R. Shahsavari, R. J.-M. Pellenq, and F.-J. Ulm, Empirical force fields for complex hydrated calcio-silicate layered materials, *Phys. Chem. Chem. Phys.* **13**, 1002 (2011).
- [87] D. Frenkel and B. Smit, *Understanding Molecular Simulation: From Algorithms to Applications* (Academic Press, New York, 2001), Vol. 1.
- [88] M. Youssef, R. J.-M. Pellenq, and B. Yildiz, Glassy nature of water in an ultraconfining disordered material: The case of calcium-silicate-hydrate, *J. Am. Chem. Soc.* **133**, 2499 (2011).
- [89] Q. Ji, R. J.-M. Pellenq, and K. J. Van Vliet, Comparison of computational water models for simulation of calcium-silicate-hydrate, *Comput. Mater. Sci.* **53**, 234 (2012).
- [90] L. J. Michot, I. Bihannic, F. Thomas, B. S. Lartiges, Y. Waldvogel, C. Caillet, J. Thieme, S. S. Funari, and P. Levitz, Coagulation of Na-montmorillonite by inorganic cations at neutral pH. A combined transmission x-ray microscopy, small angle and wide angle x-ray scattering study, *Langmuir* **29**, 3500 (2013).
- [91] E. Paineau, A. M. Philippe, K. Antonova, I. Bihannic, P. Davidson, I. Dozov, J. C. P. Gabriel, M. Impéror-Clerc, P. Levitz, F. Meneau, and L. J. Michot, Liquid-crystalline properties of aqueous suspensions of natural clay nanosheets, *Liq. Cryst. Rev.* **1**, 110 (2013).
- [92] H. F. W. Taylor and J. W. Howison, Relationships between calcium silicates and clay minerals, *Clay Miner Bull* **3**, 98 (1956).
- [93] G. Pickett, in *ACI Journal Proceedings* (ACI, 1942), Vol. 38.